Research Article

# Finite Blocklength Performance Analysis of RSMA-Based Downlink Systems with Power Beacon Energy Harvesting over Nakagami-$m$ Fading

*Quang-Sang NGUYEN*[1], *Trong-Minh HOANG*[2], *Xuan-Minh PHAM*[1], *Van Son NGUYEN*[3], *Anh Le-THI*[4], *Minh-Tuan DANG*[5], *Phu-Nguyen LE*[6,*]

[1]Posts and Telecommunications Institute of Technology, Ho Chi Minh City, Viet Nam
[2]Posts and Telecommunications Institute of Technology, HaNoi, VietNam
[3]Hanoi Open University, Hanoi, Viet Nam
[4]School of Information and Communications Technology, Hanoi University of Industry, Hanoi, VietNam
[5]Department of Microelectronics and Telecommunications, CMC University, Hanoi, VietNam
[6]Faculty of Engineering and Technology, Nguyen Tat Thanh University, Vietnam

sangnq@ptit.edu.vn, hoangtrongminh@ptit.edu.vn, minhpx@ptithcm.edu.vn, sonnv@hou.edu.vn, leanh@haui.edu.vn, dmtuan@cmcu.edu.vn, lpnguyen@ntt.edu.vn

[*]Corresponding author: Phu-Nguyen Le; lpnguyen@ntt.edu.vn

DOI: 10.15598/aeee.v24ix.250719

Article history: Received Jul 17, 2025; Revised Oct 14, 2025; Accepted Oct 20, 2025; Published Dec xx, 202x.


***Abstract.*** *Wireless energy harvesting (EH) and short-packet communications (SPC) are key technologies for enabling ultra-reliable and low-latency Internet of Things (IoT) networks. However, the performance of rate-splitting multiple access (RSMA) under finite blocklength (FBL) and energy-limited conditions remains largely unexplored. This paper develops a comprehensive analytical framework for a power beacon (PB)-assisted RSMA downlink operating over double Nakagami-m fading channels. Closed-form approximations for the block error rate (BLER) of common and private streams are derived in the FBL regime, along with high-SNR asymptotic expressions and achievable goodput analysis. Monte Carlo simulations validate the theoretical and asymptotic results, showing close agreement under various fading and power conditions. The numerical results reveal important trade-offs among blocklength, time-splitting ratio, and RSMA power allocation, and confirm that careful joint parameter optimization significantly improves reliability and throughput. These findings provide useful guidelines for designing energy-efficient and low-latency RSMA-based IoT systems.*

## Keywords

***Rate-splitting multiple access (RSMA), finite blocklength (FBL), short-packet communication (SPC), energy harvesting (EH), power beacon (PB), Nakagami-m fading, spectral efficiency***

## 1. Introduction

The exponential growth of the Internet of Things (IoT) and the global deployment of 5G/6G technologies have ushered in a new era of wireless communications [1, 2]. These emerging networks impose stringent requirements on energy efficiency, latency, and reliability to enable mission-critical applications such as industrial automation, real-time healthcare monitoring, and autonomous vehicular systems. In this context, two key enablers have attracted considerable research attention: wireless energy harvesting (EH) and short-packet communications (SPC) [3–10].

Traditional wireless systems predominantly rely on long-packet transmission and battery-powered nodes, which are unsuitable for latency-sensitive and resource-constrained IoT applications. In contrast, SPC en-

ables ultra-low latency by transmitting data blocks of only a few hundred bits. However, this benefit comes with a fundamental trade-off: the classical Shannon capacity, derived under infinite blocklength assumptions, no longer holds in this regime [9]. Instead, the achievable rate must be analyzed within the finite blocklength (FBL) framework, which explicitly captures the interplay among blocklength, reliability, and coding rate [10]. In particular, the FBL rate is lower than Shannon capacity and is strongly affected by block error rate (BLER), especially under fading channels [6, 8, 11].

Meanwhile, wireless energy harvesting (EH) has been widely studied as a sustainable solution to extend the lifetime of low-power IoT devices. In EH-enabled systems, a power beacon (PB) or an access point (AP) transfers radio-frequency (RF) energy to nearby users or relays, enabling wireless recharging and reducing the need for frequent battery replacement [3, 4]. This feature is particularly important in remote or hazardous environments where battery maintenance is difficult [5, 12]. Several EH protocols, such as power-splitting and time-switching, have been proposed to balance energy accumulation and information decoding [3,13,14]. More advanced techniques have also been investigated: for instance, self-energy recycling (S-ER) for full-duplex relays can reuse self-interference energy to improve reliability [15], while time-switching-based SWIPT protocols are optimized to enhance outage performance [16]. Furthermore, security has become a critical issue in such open networks; physical layer security (PLS) combined with multi-antenna diversity has been shown to significantly enhance resilience to eavesdropping [12, 17, 18], and secrecy outage analysis in cooperative cognitive radio networks has highlighted the impact of interference limits and hardware impairments [19].

Combining *energy harvesting (EH)* with *short-packet communications (SPC)* introduces new design challenges because energy availability is variable, and FBL transmission is more sensitive to noise and interference [6]. To cope with this, several works have proposed joint optimization of EH duration, transmit power, and blocklength. For example, Hoang *et al.* [13] investigated BLER and throughput of UAV-assisted NOMA relaying with EH under SPC, showing that optimal UAV placement and adaptive power allocation significantly enhance reliability [20]. Hybrid RF–FSO designs have also been explored for cooperative NOMA with short packets, where LAP-assisted topologies can improve link robustness in mixed fading environments [21]. Similarly, Nguyen *et al.* [22] proposed a low-complexity relaying protocol for SPC-based NOMA systems, reducing decoding complexity while maintaining reliability in cooperative settings. On the other hand, RSMA-enabled UAV communications have been analyzed under FBL and imperfect SIC conditions; Singh *et al.* [8] derived closed-form outage and throughput expressions, providing useful insights for practical RSMA applications [23]. More recently, Tan *et al.* [24] integrated reconfigurable intelligent surfaces (RISs) into full-duplex cooperative systems and demonstrated that RIS-assisted relay networks can improve reliability and mitigate residual self-interference, which is particularly promising for EH–SPC scenarios.

Parallel to the progress in EH and SPC, rate-splitting multiple access (RSMA) has emerged as a flexible strategy for improving both spectral and energy efficiency in multi-user wireless networks. Unlike conventional multiple access schemes such as NOMA or OMA, RSMA splits each user's message into common and private parts, enabling partial interference decoding and adaptive interference management [25]. This feature allows RSMA to outperform traditional schemes not only under various CSI and fairness constraints [26] but also in short-packet transmissions, where it achieves comparable BLER to NOMA with significantly shorter blocklength [11]. Its robustness to imperfect CSI and reduced SIC complexity make RSMA particularly suitable for latency-sensitive and energy-constrained systems [8, 27]. Additionally, RIS-aided RSMA designs have been investigated to further improve energy and spectral efficiency; Katwe *et al.* [26] proposed a RIS-assisted RSMA framework for mobile broadband reliable low-latency communications (mBRLLC), while Tan *et al.* [28] analyzed RIS–relay integration to enhance outage probability and symbol error rate in IoT-oriented LPWA networks over Nakagami-$m$ fading channels.

However, most existing studies on RSMA still rely on the assumption of infinite blocklength coding, limiting their applicability in URLLC or IoT scenarios where short-packet transmission dominates [8]. Only a few recent works have analyzed RSMA under FBL constraints. For example, Zhang *et al.* [11] derived closed-form expressions for the blocklength required to guarantee URLLC reliability in uplink RSMA, while Nguyen *et al.* [27] evaluated RSMA-enabled UAV systems with imperfect SIC, confirming its robustness under realistic CSI conditions. Despite these advances, the integration of RSMA with EH remains underexplored. Recent studies in EH-powered systems have primarily focused on NOMA or relay-based approaches [6, 15, 16, 24], but no existing work has provided a unified theoretical framework for RSMA under FBL and EH constraints, particularly over realistic Nakagami-$m$ fading channels.

Unlike conventional NOMA–EH systems that depend exclusively on power-domain multiplexing and are highly sensitive to imperfect SIC and short-packet constraints, RSMA–FBL provides an additional degree of freedom through message splitting and joint de-

coding. This enables better interference management and reliability preservation even when the transmission blocklength and harvested energy are limited. Therefore, the proposed RSMA–FBL design fundamentally differs from NOMA–EH in terms of both interference control and finite-blocklength adaptability.

Motivated by these observations, this paper develops a unified analytical framework for RSMA-powered short-packet communications in energy-constrained IoT networks. We consider a power beacon-assisted RSMA downlink operating over double Nakagami-$m$ fading channels, where the access point relies entirely on harvested energy for data transmission. Closed-form expressions for the block error rate (BLER) and achievable goodput are derived under the FBL regime, together with high-SNR asymptotic approximations. The proposed analysis explicitly characterizes the interplay among energy harvesting time, blocklength, and RSMA power allocation, offering practical design insights into the reliability–latency trade-offs under realistic fading and energy constraints. Numerical simulations validate the theoretical and asymptotic results, revealing optimal configurations for the time-splitting ratio, blocklength, and power coefficients that significantly enhance reliability and throughput in energy-limited short-packet RSMA systems.

The key contributions of this paper are summarized as follows:

1. **RSMA-powered short-packet transmission under wireless energy harvesting:** We propose a novel downlink framework that integrates rate-splitting multiple access (RSMA) with power beacon-enabled energy harvesting (PB-EH) for short-packet communications (SPC) over Nakagami-$m$ fading channels. To the best of our knowledge, this is the first theoretical study that jointly addresses RSMA, finite blocklength coding, and dedicated EH in a unified framework.

2. **Analytical performance characterization under finite blocklength:** We derive closed-form expressions for key performance metrics, including average block error rate (BLER), goodput, and their asymptotic behaviors in the high-SNR regime. These expressions capture the coupling between EH duration, RSMA power allocation, and finite blocklength constraints, providing fundamental insights into reliability–latency trade-offs.

3. **Design insights through extensive numerical validation:** Monte Carlo simulations confirm the accuracy of the theoretical and asymptotic analyses. The results systematically illustrate how Nakagami fading severity, PB transmit power, EH time allocation, blocklength, and RSMA power-splitting coefficients affect BLER and goodput. Furthermore, joint optimization of time-switching ratio and blocklength is shown to significantly improve reliability in energy-constrained short-packet scenarios.

The rest of this paper is organized as follows. Section 2. introduces the system and channel models. Section 3. presents the theoretical derivation of average BLER, goodput, and high-SNR approximations. Section 4. discusses simulation results and design implications. Section 5. concludes the paper.

## 2. System Model

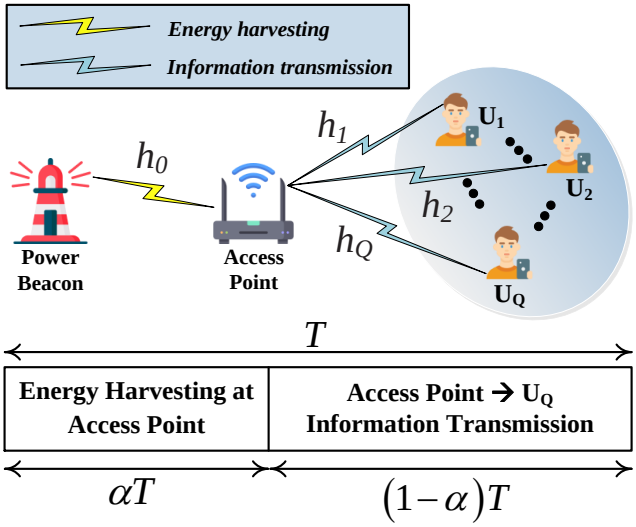


**Fig. 1:** System model of a power beacon-assisted RSMA downlink transmission.

We consider a power beacon (PB)-assisted downlink communication system that integrates wireless energy transfer (WET) and rate-splitting multiple access (RSMA), as illustrated in Fig. 1. The network comprises a dedicated PB, a wireless access point (AP), and a set of $Q$ single-antenna users denoted by $\{U_1, U_2, \ldots, U_Q\}$. All nodes operate over a common frequency band and are equipped with a single antenna.

The PB continuously transmits radio frequency (RF) energy to the AP, which lacks a conventional energy source and relies solely on harvested power for information transmission. The wireless link from the PB to the AP is characterized by channel coefficient $h_0$, while the channel from the AP to user $U_q$ is denoted by $h_q$, for $q = 1, 2, \ldots, Q$. All channels experience frequency-flat, quasi-static block fading, where the fading remains constant over a transmission block of duration $T$ and changes independently across blocks. Each channel coefficient is modeled as a Nakagami-$m$ random variable,

and perfect channel state information (CSI) is assumed to be available at all receiving nodes.

Each transmission block $T$ is divided into two phases. During the energy harvesting phase of duration $\alpha T$ $(0 \leq \alpha \leq 1)$, the AP harvests energy from the PB. In the subsequent $(1-\alpha)T$ phase, the AP utilizes the harvested energy to transmit data to users. The amount of harvested energy at the AP is given by

$$E_{\mathrm{h}}^{\mathrm{AP}} = \eta \alpha T P_{\mathrm{PB}} |h_0|^2, \tag{1}$$

where $P_{\mathrm{PB}}$ denotes the transmit power of the PB, $|h_0|^2$ is the channel power gain between PB and AP, and $\eta \in (0, 1]$ is the energy conversion efficiency at the AP.

Assuming that the AP fully utilizes the harvested energy for downlink transmission, the transmit power of the AP is determined as

$$P_{\mathrm{AP}} = \frac{E_{\mathrm{h}}^{\mathrm{AP}}}{(1-\alpha)T} = \frac{\eta \alpha P_{\mathrm{PB}} |h_0|^2}{1-\alpha}. \tag{2}$$

Following the RSMA principle, the AP transmits a superimposed signal comprising a common message $s_c$ intended for all users, and private messages $\{s_1, \ldots, s_Q\}$ intended for each specific user. The transmit signal is expressed as

$$s = \sqrt{a_c} s_c + \sum_{q=1}^{Q} \sqrt{a_q} s_q, \tag{3}$$

where $a_c$ and $\{a_q\}$ represent the power allocation coefficients for the common and private messages, respectively, satisfying $a_c + \sum_{q=1}^{Q} a_q = 1$.

The received signal at user $U_q$ is given by

$$\begin{aligned} y_{U_q} &= h_q \sqrt{P_{\mathrm{AP}}} s + n_{U_q} \\ &= \underbrace{\sqrt{a_c P_{\mathrm{AP}}} h_q s_c}_{\text{common message}} + \underbrace{\sqrt{a_q P_{\mathrm{AP}}} h_q s_q}_{\text{desired private message}} \\ &\quad + \underbrace{\sum_{j \neq q} \sqrt{a_j P_{\mathrm{AP}}} h_q s_j}_{\text{multi-user interference}} + \underbrace{n_{U_q}}_{\text{AWGN}}, \end{aligned} \tag{4}$$

where $n_{U_q} \sim \mathcal{CN}(0, N_0)$ denotes the additive white Gaussian noise (AWGN) at user $U_q$.

Each user applies a two-stage successive interference cancellation (SIC) decoding procedure. First, the common message $s_c$ is decoded while treating all private messages as interference. The corresponding signal-to-interference-plus-noise ratio (SINR) at user $U_q$ is given by

$$S_{c,q} = \frac{a_c P_{\mathrm{AP}} |h_q|^2}{(1-a_c) P_{\mathrm{AP}} |h_q|^2 + N_0}. \tag{5}$$

By substituting (2) into (5), we obtain a compact SINR expression:

$$S_{c,q} = \frac{\phi_2 \mathcal{A}_q}{\phi_1 \mathcal{A}_q + 1}, \tag{6}$$

where $\mathcal{A}_q = |h_0|^2 |h_q|^2$ represents the cascaded channel gain from PB to AP and then to user $U_q$, $\rho = P_{\mathrm{PB}}/N_0$ is the reference signal-to-noise ratio (SNR), and

$$\phi_1 = \frac{(1-a_c)\eta\alpha\rho}{1-\alpha}, \quad \phi_2 = \frac{a_c \eta \alpha \rho}{1-\alpha}.$$

Upon successful decoding and removal of the common message, user $U_q$ proceeds to decode its intended private message $s_q$, treating the other users' private messages as interference. The resulting SINR is given by

$$S_{p,q} = \frac{\phi_{4,q} \mathcal{A}_q}{\phi_{3,q} \mathcal{A}_q + 1}, \tag{7}$$

where

$$\phi_{3,q} = \frac{\eta\alpha\rho \sum_{j \neq q} a_j}{1-\alpha}, \quad \phi_{4,q} = \frac{a_q \eta \alpha \rho}{1-\alpha}.$$

The above expressions clearly show that the system performance is governed by the joint effect of the channel gains, power allocation strategy, and the time-splitting parameter $\alpha$.

Table 1 summarizes the key notations and system parameters used throughout the paper.

**Tab. 1:** Summary of key system parameters and notations.

| Symbol | Description |
|---|---|
| $a_c$ | Power allocation coefficient for the common message |
| $a_q$ | Power allocation coefficient for the private message intended for user $U_q$ |
| $s_c$ | Common message intended for all users |
| $s_q$ | Private message intended for user $U_q$ |
| $L_c$ | Blocklength allocated to the common message |
| $L_p$ | Blocklength allocated to the private messages |
| $B_c, B_q$ | Number of information bits in the common and private messages, respectively |
| $P_{\mathrm{AP}}$ | Transmit power at the access point (AP) |
| $P_{\mathrm{PB}}$ | Transmit power at the power beacon (PB) |
| $T$ | Total block duration |
| $\eta$ | Energy conversion efficiency at the AP |
| $\alpha$ | Time-splitting ratio between energy harvesting and data transmission |
| $h_0$ | Channel coefficient from PB to AP |
| $h_q$ | Channel coefficient from AP to user $U_q$ |

**Remark 1:** In this work, perfect channel state information (CSI) is assumed at the receivers and the access point to focus on the effects of finite blocklength and energy harvesting. As discussed in [8], imperfect CSI mainly introduces residual interference in successive interference cancellation (SIC), leading to slightly higher BLER and reduced goodput. Extending the present

framework to include channel estimation errors under imperfect CSI will be an interesting direction for future research.

**Remark 2:** The proposed framework, developed for double Nakagami-$m$ fading, is general enough to capture other fading scenarios. In particular, Rayleigh fading corresponds to $m = 1$, while Rician fading can be approximated by moderate $m$ values associated with the Rician $K$-factor. Hence, the derived analytical expressions can be readily adapted to different fading conditions without altering the overall derivation structure.

# 3. Finite Blocklength Analysis

In this section, we analyze the performance of the proposed RSMA-enabled wireless system in the finite blocklength (FBL) regime. Unlike the classical Shannon capacity framework which assumes infinite-length codewords, FBL analysis characterizes the trade-off between latency, reliability, and rate — making it suitable for ultra-reliable low-latency communication (URLLC) and massive IoT scenarios.

## 3.1. Channel Characterization: Double Nakagami-$m$ Model

To accurately capture the joint randomness in energy harvesting and information transmission, we adopt a composite fading model where the end-to-end link is characterized as the product of two independent Nakagami-$m$ channels:

- The first hop, from the power beacon (PB) to the access point (AP), has channel gain $|h_0|^2$;
- The second hop, from the AP to user $U_q$, has gain $|h_q|^2$.

Both $|h_0|^2$ and $|h_q|^2$ are modeled as Gamma-distributed random variables, a natural consequence of the Nakagami-$m$ fading assumption. Consequently, the equivalent end-to-end channel gain is given by:

$$\mathcal{A}_q = |h_0|^2 \cdot |h_q|^2, \tag{8}$$

which represents the product of two independent Gamma random variables.

This leads to what is known as the *double Nakagami-m fading model*, which generalizes a wide range of propagation scenarios:

- If $m_0 = m_q = 1$, the distribution reduces to the double Rayleigh fading model;
- If $m_0 = m_q = 0.5$, it becomes the double one-sided Gaussian distribution;
- As $m_0$, $m_q$ increase, the channel becomes more deterministic and less prone to deep fades.

The exact characterization of the distribution of $\mathcal{A}_q$ is essential for evaluating the reliability performance under FBL. This distribution can be expressed in closed-form using the Meijer-G function — a versatile class of special functions that naturally arise in the product of Gamma variables.

**Proposition 1.** *Let $|h_0|^2 \sim Gamma(m_0, \lambda_0/m_0)$ and $|h_q|^2 \sim Gamma(m_q, \lambda_q/m_q)$ denote the squared amplitudes of independent Nakagami-m fading channels. Then, the PDF and CDF of the end-to-end channel gain $\mathcal{A}_q = |h_0|^2 \cdot |h_q|^2$ are given by:*

$$f_{\mathcal{A}_q}(x) = \frac{1}{x\,\Gamma(m_0)\Gamma(m_q)} G_{0,2}^{2,0}\left(\frac{m_0 m_q}{\lambda_0 \lambda_q} x \,\middle|\, -; m_0, m_q\right), \tag{9}$$

$$F_{\mathcal{A}_q}(x) = \frac{1}{\Gamma(m_0)\Gamma(m_q)} G_{1,3}^{2,1}\left(\frac{m_0 m_q}{\lambda_0 \lambda_q} x \,\middle|\, 1; m_0, m_q, 0\right). \tag{10}$$

Here, $\Gamma(\cdot)$ denotes the Gamma function and $G_{p,q}^{m,n}(\cdot)$ is the Meijer-G function. These expressions will serve as the basis for the BLER and goodput derivations in the following subsections.

**Remark 1.** *The double Nakagami-m model effectively captures the compounding uncertainties in wireless-powered communication systems, where both energy and data links are subject to fading. Its analytical tractability through the Meijer-G function makes it suitable for FBL performance evaluation, enabling closed-form expressions for reliability and throughput metrics.*

## 3.2. Reliability Analysis under Finite Blocklength Regime

Conventional channel coding theory typically assumes infinite blocklengths, where decoding errors vanish asymptotically. However, emerging applications such as URLLC and massive IoT necessitate transmission of short packets, where such assumptions are no longer valid. This motivates the study of performance under the finite blocklength (FBL) regime.

According to [9], the maximum coding rate achievable at user $U_1$ under finite blocklength $L_q$, SINR $\gamma_q$, and target BLER $\epsilon_q$ is approximated by:

$$r_{U_1}(L_q,\gamma_q,\epsilon_q) \approx \mathcal{C}(\gamma_q) - \sqrt{\frac{\mathcal{V}(\gamma_q)}{L_q}}\,\mathcal{Q}^{-1}(\epsilon_q) + \mathcal{O}\left(\frac{\log_2 L_q}{L_q}\right), \tag{11}$$

where:

- $\mathcal{C}(\gamma_q) = \log_2(1+\gamma_q)$ is the Shannon capacity;
- $\mathcal{V}(\gamma_q) = \left[1-(1+\gamma_q)^{-2}\right](\log_2 e)^2$ is the channel dispersion;
- $\mathcal{Q}^{-1}(\cdot)$ is the inverse Gaussian Q-function;
- The residual term $\mathcal{O}(\cdot)$ is negligible for $L_q \geq 100$.

**1) Instantaneous and Average BLER for the Common Stream:**

Using (11), the instantaneous BLER when decoding the common message at user $U_q$ is:

$$\epsilon_{c,q} \approx \mathcal{Q}\left(\frac{\mathcal{C}(S_{c,q}) - r_c}{\sqrt{\mathcal{V}(S_{c,q})/[L_c(1-\alpha)]}}\right), \tag{12}$$

where $r_c = \frac{B_c}{L_c(1-\alpha)}$ and $S_{c,q}$ is the instantaneous SINR for the common message. Averaging (12) over the fading distribution yields:

$$\tilde{\epsilon}_{c,q} = \mathbb{E}_{S_{c,q}}[\epsilon_{c,q}]. \tag{13}$$

To approximate (13), we adopt a linear Q-function approximation [7]:

$$\Xi_{c,q}(x) = \begin{cases} 1, & x \leq \vartheta_c \\ 0.5 - \chi_c(x-\gamma_c), & \vartheta_c < x < \psi_c \\ 0, & x \geq \psi_c \end{cases}, \tag{14}$$

where:

$$\gamma_c = 2^{r_c} - 1,$$
$$\chi_c = \left[\frac{2\pi(2^{2r_c}-1)}{L_c(1-\alpha)}\right]^{-1/2},$$
$$\vartheta_c = \gamma_c - \frac{1}{2\chi_c}, \quad \psi_c = \gamma_c + \frac{1}{2\chi_c}.$$

Then:

$$\tilde{\epsilon}_{c,q} \approx \int_{\vartheta_c}^{\psi_c} \chi_c F_{S_{c,q}}(x)dx, \tag{15}$$

with $F_{S_{c,q}}(x)$ being the CDF of $S_{c,q}$. Under double Nakagami-$m$ fading:

$$F_{S_{c,q}}(x) = \frac{1}{\Gamma(m_0)\Gamma(m_q)} G_{1,3}^{2,1}\left(\frac{m_0 m_q \Delta_q(x)}{\lambda_0\lambda_q}\,\middle|\,\begin{matrix}1\\ m_0, m_q, 0\end{matrix}\right), \tag{16}$$

where $\Delta_q(x) = \frac{x}{\phi_2 - \phi_1 x}$. Applying the midpoint rule:

$$\tilde{\epsilon}_{c,q} \approx \frac{\chi_c(\psi_c+\vartheta_c)}{\Gamma(m_0)\Gamma(m_q)} G_{1,3}^{2,1}\left(\frac{m_0 m_q \Delta_q\left(\frac{\psi_c+\vartheta_c}{2}\right)}{\lambda_0\lambda_q}\,\middle|\,\begin{matrix}1\\ m_0, m_q, 0\end{matrix}\right). \tag{17}$$

**2) Average BLER for the Private Stream:**

Applying the same procedure for the private message, the instantaneous BLER is:

$$\epsilon_{p,q} \approx \mathcal{Q}\left(\frac{\mathcal{C}(S_{p,q}) - r_p}{\sqrt{\mathcal{V}(S_{p,q})/[L_p(1-\alpha)]}}\right), \tag{18}$$

where $r_p = \frac{B_p}{L_p(1-\alpha)}$ and $S_{p,q}$ is the SINR of the private stream. The average BLER is:

$$\tilde{\epsilon}_{p,q} = \mathbb{E}_{S_{p,q}}[\epsilon_{p,q}]. \tag{19}$$

We apply the Q-function approximation:

$$\Xi_{p,q}(x) = \begin{cases} 1, & x \leq \vartheta_p \\ 0.5 - \chi_p(x-\gamma_p), & \vartheta_p < x < \psi_p \\ 0, & x \geq \psi_p \end{cases}, \tag{20}$$

with:

$$\gamma_p = 2^{r_p} - 1,$$
$$\chi_p = \left[\frac{2\pi(2^{2r_p}-1)}{L_p(1-\alpha)}\right]^{-1/2},$$
$$\vartheta_p = \gamma_p - \frac{1}{2\chi_p}, \quad \psi_p = \gamma_p + \frac{1}{2\chi_p}.$$

Therefore:

$$\tilde{\epsilon}_{p,q} \approx \chi_p \int_{\vartheta_p}^{\psi_p} F_{S_{p,q}}(x)dx, \tag{21}$$

where $F_{S_{p,q}}(x)$ is the CDF of the SINR under composite fading:

$$F_{S_{p,q}}(x) = \frac{1}{\Gamma(m_0)\Gamma(m_q)} G_{1,3}^{2,1}\left(\frac{m_0 m_q \Delta_p(x)}{\lambda_0\lambda_q}\,\middle|\,\begin{matrix}1\\ m_0, m_q, 0\end{matrix}\right), \tag{22}$$

where $\Delta_p(x) = \frac{x}{\phi_{4,q} - \phi_{3,q}x}$ and is valid for $x < \phi_{4,q}/\phi_{3,q}$.

Using the midpoint approximation, the average BLER becomes:

$$\tilde{\epsilon}_{p,q} \approx \frac{\chi_p(\psi_p+\vartheta_p)}{\Gamma(m_0)\Gamma(m_q)} G_{1,3}^{2,1}\left(\frac{m_0 m_q \Delta_p\left(\frac{\psi_p+\vartheta_p}{2}\right)}{\lambda_0\lambda_q}\middle| \begin{matrix}1\\ m_0, m_q, 0\end{matrix}\right). \tag{23}$$

**3) Total Average BLER and Closed-Form Approximation:**

The total block error rate (BLER) for user $U_q$ reflects the combined reliability of decoding both the common and private messages. It is defined as the arithmetic mean of the respective BLERs:

$$\tilde{\epsilon}_q = \frac{1}{2}\left(\tilde{\epsilon}_{c,q} + \tilde{\epsilon}_{p,q}\right). \tag{24}$$

By substituting the closed-form approximations from (17) and (23), we derive the following unified expression:

$$\tilde{\epsilon}_q \approx \frac{1}{2\,\Gamma(m_0)\Gamma(m_q)}\Bigg[ \frac{G_{1,3}^{2,1}\left(\frac{m_0 m_q \Delta_q\left(\frac{\psi_c+\vartheta_c}{2}\right)}{\lambda_0\lambda_q}\middle| \begin{matrix}1\\ m_0, m_q, 0\end{matrix}\right)}{\chi_c(\psi_c+\vartheta_c)^{-1}} + \frac{G_{1,3}^{2,1}\left(\frac{m_0 m_q \Delta_p\left(\frac{\psi_p+\vartheta_p}{2}\right)}{\lambda_0\lambda_q}\middle| \begin{matrix}1\\ m_0, m_q, 0\end{matrix}\right)}{\chi_p(\psi_p+\vartheta_p)^{-1}}\Bigg]. \tag{25}$$

This expression consolidates the average reliability for each user and admits fast evaluation due to the closed-form nature of the Meijer-G function.

**4) Network-Wide BLER:**

To quantify overall network reliability, the average BLER across all $Q$ users is computed as:

$$\tilde{\epsilon}_o = \frac{1}{Q}\sum_{q=1}^{Q}\tilde{\epsilon}_q. \tag{26}$$

This metric captures the expected block-level reliability for the RSMA system under finite blocklength constraints and double Nakagami-$m$ fading channels.

**5) Achievable Goodput:**

The average goodput of user $U_q$, denoted by $\mathbb{G}_q$, reflects the average number of successfully delivered bits per channel use and is defined as:

$$\mathbb{G}_q = \left(1 - \frac{L_c(1-\alpha) - B_c}{L_c(1-\alpha)}\right)\hat{R}_c \cdot (1-\hat{\epsilon}_{c,q}) + \left(1 - \frac{L_p(1-\alpha) - B_p}{L_p(1-\alpha)}\right)\hat{R}_{p,q} \cdot (1-\hat{\epsilon}_{p,q}), \tag{27}$$

where:

- $\hat{R}_c = \frac{B_c}{L_c(1-\alpha)}$ and $\hat{R}_{p,q} = \frac{B_p}{L_p(1-\alpha)}$ are the effective target coding rates;
- $\hat{\epsilon}_{c,q}$ and $\hat{\epsilon}_{p,q}$ are obtained using the approximations in (17) and (23) by substituting $r_c = \hat{R}_c$ and $r_p = \hat{R}_{p,q}$.

The total network goodput is then expressed as:

$$\mathbb{G}_o = \sum_{q=1}^{Q}\mathbb{G}_q. \tag{28}$$

## 3.3. High SNR Regime Analysis

In practical wireless communication systems, analyzing the high signal-to-noise ratio (SNR) regime provides valuable insights into the asymptotic reliability behavior when transmission power becomes abundant. In this regime, closed-form approximations of the average block error rate (BLER) become tractable and insightful, especially under composite fading.

**1) Asymptotic Expansion of Meijer G-Function:**

The Meijer G-function appears in the closed-form BLER expressions for both the common and private streams. According to the asymptotic result from [21, Eq. (18)], for large arguments $z \to \infty$, the Meijer G-function can be approximated as:

$$G_{p,q}^{m,n}\left(z\middle| \begin{matrix}a_1,\ldots,a_p\\ b_1,\ldots,b_q\end{matrix}\right) \approx \sum_{k=1}^{m}\frac{\prod_{\substack{j=1\\ j\neq k}}^{m}\Gamma(b_j-b_k)\prod_{j=1}^{n}\Gamma(1-a_j+b_k)}{\prod_{j=n+1}^{p}\Gamma(a_j-b_k)\prod_{j=m+1}^{q}\Gamma(1-b_j+b_k)}\cdot z^{b_k}. \tag{29}$$

This expansion is instrumental in deriving the asymptotic forms of BLER as $\rho \to \infty$.

**2) Asymptotic BLER under High SNR Regime:**

In the high signal-to-noise ratio (SNR) regime, i.e., as $\rho \to \infty$, the Meijer G-functions appearing in the average BLER expressions can be approximated using the

asymptotic expansion in (29). This leads to tractable closed-form representations of the average BLERs for both the common and private streams.

By applying the expansion in (29) to the BLER expressions (17) and (23), we obtain the asymptotic BLER for the common stream $\tilde{\epsilon}_{c,q}^{\infty}$ and for the private stream $\tilde{\epsilon}_{p,q}^{\infty}$, respectively. These are shown in (30) and (31), where the expressions depend on the relative values of the Nakagami fading parameters $m_0$ and $m_q$.

## 4. Numerical Results

In this section, we present numerical results to validate the theoretical and asymptotic analyses derived in Section 3. . Monte Carlo simulations [29–32] are carried out over $10^6$ realizations. The main system parameters are summarized in Table 2. Unless otherwise stated, the system assumes $Q = 3$ users with uniform power allocation for the private streams, i.e., $a_1 = a_2 = a_3 = \frac{1-a_c}{3}$, and symmetric fading parameters $m = m_0 = m_1 = m_2 = m_3$.

**Tab. 2:** System parameters used in simulations

| **Parameter (Notation)** | **Value** |
|---|---|
| Monte Carlo realizations | $10^6$ |
| Common-message power coefficient ($a_c$) | 0.5 |
| Fading parameter ($m$) | 3 (varies) |
| Blocklength ($L_c = L_p$) | 350 (varies) |
| Information bits ($B_c = B_p$) | 75 |
| Energy conversion efficiency ($\eta$) | 0.8 |
| Time-splitting ratio ($\alpha$) | 0.2 (varies) |
| Exponential parameters ($\lambda_0, \lambda_1, \lambda_2, \lambda_3$) | $\lambda_0 = 1$, $\lambda_1 = 0.2$, $\lambda_2 = 0.4$, $\lambda_3 = 0.6$ |

Unless otherwise stated, the common-stream power coefficient is set to $a_c = 0.5$, which provides a balanced power allocation between the common and private messages and ensures fair decoding reliability among users.

The simulation results are obtained based on the exact finite blocklength expressions in Eqs. (12) and (18) for the common and private messages, respectively. The corresponding theoretical approximations are evaluated via Eqs. (17) and (22), while the high-SNR asymptotic expressions for both streams are derived from Eqs. (29) and (30).

Figure 2 illustrates the average block error rate (BLER) performance as a function of the power beacon transmit power $\rho$ (in dB), under various values of the Nakagami-$m$ fading parameter. The left subfigure shows the per-user average BLER for three users, while the right subfigure presents the overall average BLER. Both theoretical and asymptotic curves are compared with Monte Carlo simulation results.

It is evident that the average BLER decreases as $\rho$ increases, which is expected due to enhanced energy harvesting and stronger downlink transmission power. Moreover, for a given $\rho$, larger values of the fading parameter $m$ yield significantly better BLER performance. This is because higher $m$ corresponds to less severe fading, reducing channel randomness in both the energy and data links.

The theoretical curves, computed from Eqs. (17) and (22), closely match the simulation results across all users and fading conditions. Furthermore, the asymptotic curves based on Eq. (30) also align well in the high-SNR regime, validating the high-SNR analysis framework developed in Section 3. .

This figure confirms that the proposed RSMA-based system under double Nakagami-$m$ fading is both analytically tractable and practically robust, especially in high-$m$ or high-$\rho$ scenarios.

Figure 3 investigates how the time-splitting ratio $\alpha$ influences the reliability performance under two different PB transmit power levels: $\rho = 20$ dB and $\rho = 30$ dB, with the fading parameter set to $m = 3$. All curves are obtained from Monte Carlo simulations.

The results show that each user experiences a non-monotonic response to changes in $\alpha$. This is due to the inherent trade-off between the duration allocated to energy harvesting and the time left for information transmission. At low values of $\alpha$, the harvested energy is insufficient to support high-quality transmission, whereas at high $\alpha$, the available blocklength becomes too short to ensure reliable decoding.

As the PB power increases, the optimal $\alpha$ shifts to smaller values, indicating that stronger external energy allows for more aggressive allocation of time toward data transmission. This adaptability is a key strength of RSMA-based wireless-powered systems, where optimal configuration depends jointly on system power availability and latency constraints.

In contrast to Figure 2, where fading severity ($m$) was the main variable, this figure emphasizes the impact of time-domain resource allocation under fixed channel statistics. The insights here guide practical selection of $\alpha$ to balance energy acquisition and spectral efficiency.

Figure 4 illustrates the overall average BLER as a function of the blocklength ($L_c = L_p$), under different PB transmit power levels $\rho$, with the fading parameter fixed at $m = 3$ and time-splitting ratio $\alpha$ held constant.

As expected, increasing the blocklength consistently improves system reliability. Longer codewords en-

$$\tilde{\epsilon}_{c,q}^{\infty} \approx \begin{cases} \dfrac{\chi_c(\psi_c+\vartheta_c)\Gamma(m_0-m_q)}{\Gamma(m_q)\Gamma(m_0)m_q}\left(\dfrac{m_0 m_q}{\lambda_0\lambda_q}\Delta_q\left(\dfrac{\psi_c+\vartheta_c}{2}\right)\right)^{m_q}, & \text{if } m_0 > m_q, \\ \dfrac{\chi_c(\psi_c+\vartheta_c)\Gamma(m_q-m_0)}{\Gamma(m_0)\Gamma(m_q)m_0}\left(\dfrac{m_0 m_q}{\lambda_0\lambda_q}\Delta_q\left(\dfrac{\psi_c+\vartheta_c}{2}\right)\right)^{m_0}, & \text{if } m_0 < m_q, \\ -\dfrac{\chi_c(\psi_c+\vartheta_c)}{m\Gamma^2(m)}\ln\left(\dfrac{m^2}{\lambda_0\lambda_q}\Delta_q\left(\dfrac{\psi_c+\vartheta_c}{2}\right)\right)\left(\dfrac{m^2}{\lambda_0\lambda_q}\Delta_q\left(\dfrac{\psi_c+\vartheta_c}{2}\right)\right)^{m}, & \text{if } m_0 = m_q = m. \end{cases} \tag{30}$$

$$\tilde{\epsilon}_{p,q}^{\infty} \approx \begin{cases} \dfrac{\chi_p(\psi_p+\vartheta_p)\Gamma(m_0-m_q)}{\Gamma(m_q)\Gamma(m_0)m_q}\left(\dfrac{m_0 m_q}{\lambda_0\lambda_q}\Delta_p\left(\dfrac{\psi_p+\vartheta_p}{2}\right)\right)^{m_q}, & \text{if } m_0 > m_q, \\ \dfrac{\chi_p(\psi_p+\vartheta_p)\Gamma(m_q-m_0)}{\Gamma(m_0)\Gamma(m_q)m_0}\left(\dfrac{m_0 m_q}{\lambda_0\lambda_q}\Delta_p\left(\dfrac{\psi_p+\vartheta_p}{2}\right)\right)^{m_0}, & \text{if } m_0 < m_q, \\ -\dfrac{\chi_p(\psi_p+\vartheta_p)}{m\Gamma^2(m)}\ln\left(\dfrac{m^2}{\lambda_0\lambda_q}\Delta_p\left(\dfrac{\psi_p+\vartheta_p}{2}\right)\right)\left(\dfrac{m^2}{\lambda_0\lambda_q}\Delta_p\left(\dfrac{\psi_p+\vartheta_p}{2}\right)\right)^{m}, & \text{if } m_0 = m_q = m. \end{cases} \tag{31}$$

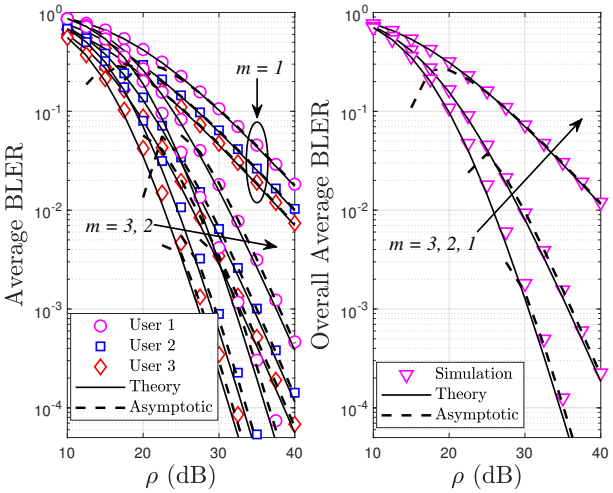


**Fig. 2:** Average and overall block error rate (BLER) versus PB transmit power $\rho$ for different Nakagami-$m$ fading parameters, with $Q = 3$ users. Left: per-user BLER. Right: overall average BLER.

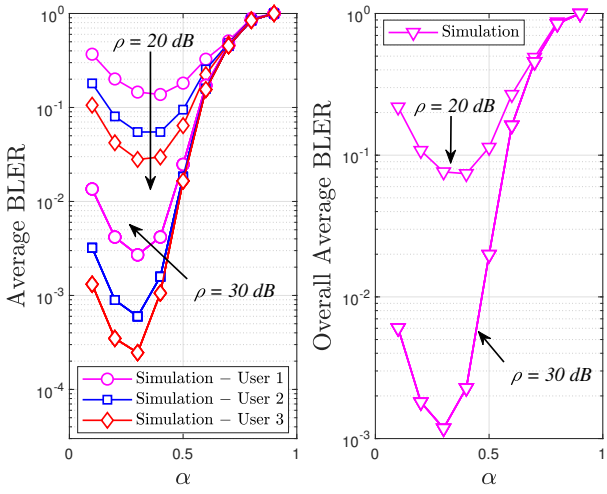


**Fig. 3:** Average BLER and overall average BLER versus time switching ratio $\alpha$ for different transmit power levels of PB, with $m = 3$.

hance error-correcting capability and reduce the effect of finite-length penalties, in agreement with the finite blocklength approximation given in Eq. (11). This effect is especially pronounced when $\rho$ is low, where the system relies heavily on coding gain to compensate for limited transmit power.

At higher $\rho$ values, the system achieves lower BLER across all blocklengths. Interestingly, even with moderate blocklengths (e.g., $L = 200$–$250$), the BLER drops below $10^{-3}$ when $\rho \geq 30$ dB, highlighting that sufficient energy provisioning can partly offset the limitations imposed by short packets.

Unlike Figure 3, which emphasized the impact of $\alpha$, this figure focuses solely on the coding dimension and shows that proper selection of blocklength—tailored to system power and reliability requirements—is crucial in URLLC and energy-constrained applications.

Figure 5 presents a three-dimensional surface plot of the overall average BLER as a function of both blocklength ($L_c = L_p$) and the time-splitting ratio $\alpha$, with fixed system parameters $m = 2$ and $\rho = 20$ dB.

The surface clearly exhibits a convex structure with respect to both variables. As the blocklength increases, the BLER decreases due to improved channel coding efficiency, consistent with the finite blocklength analysis from Eq. (11). Simultaneously, varying $\alpha$ reveals a classic trade-off: a low $\alpha$ results in insufficient harvested energy (hence low transmit power), while a high $\alpha$ leaves little time for data transmission, especially problematic under short-packet constraints.

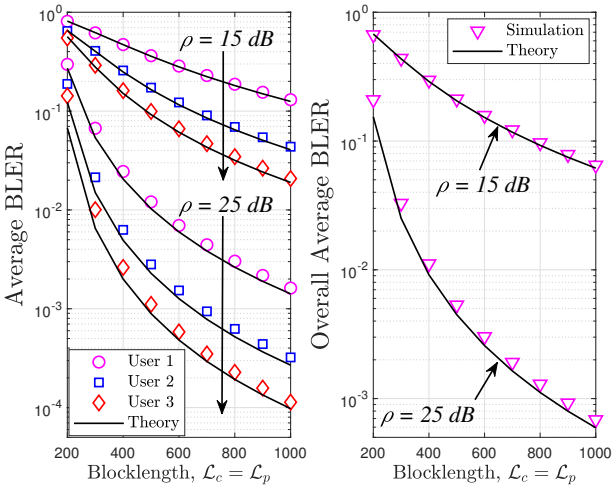


**Fig. 4:** Overall average BLER versus blocklength $\mathcal{L}_c = \mathcal{L}_p$ for different PB transmit power levels $\rho$, with $m = 3$ and fixed $\alpha$.

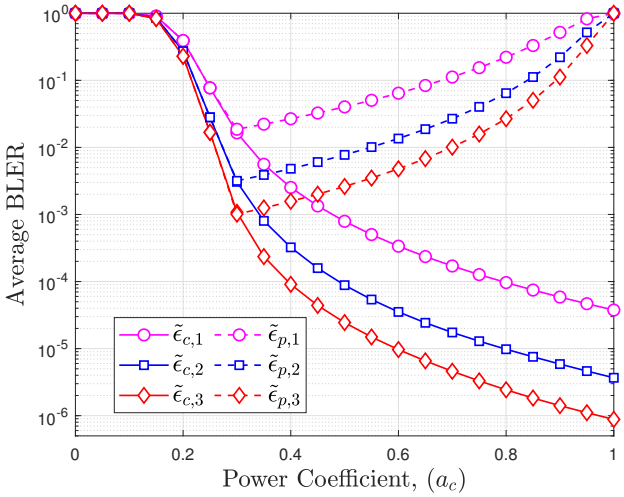


**Fig. 6:** Average BLER versus power coefficient $(a_c)$, with $m = 4$ and $\rho = 25$ dB.

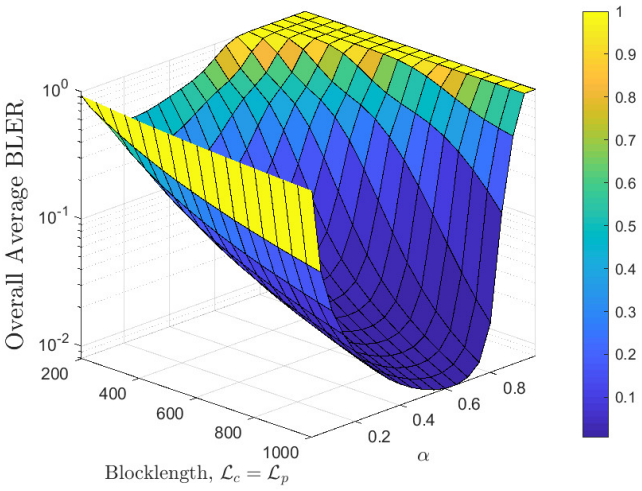


**Fig. 5:** Overall average BLER versus blocklength $\mathcal{L}_c = \mathcal{L}_p$ and time switching ratio $\alpha$, with $m = 2$ and $\rho = 20$ dB.

The presence of a well-defined minimum on the surface confirms that a jointly optimal pair $(L^*, \alpha^*)$ exists to minimize BLER. Notably, this joint optimality is not achievable by tuning $L$ or $\alpha$ independently. Hence, the result emphasizes the need for joint optimization of physical-layer and protocol-level parameters in RSMA systems operating under energy and latency constraints.

Compared to Figures 3 and 4, which varied $\alpha$ or $L$ individually, this figure visualizes the full two-dimensional interaction and reveals a deeper design space for low-BLER operation.

Figure 6 illustrates the relationship between the power allocation coefficient of the common message, $a_c$, and the average block error rate (BLER) for each user in both the common and private streams. The channel fading parameter is set to $m = 4$, and the power beacon transmit power is fixed at $\rho = 25$ dB.

Each solid curve represents the average BLER $\tilde{\epsilon}_{c,q}$ for the common message decoded by user $q$, while each dashed curve corresponds to the private stream BLER $\tilde{\epsilon}_{p,q}$. As $a_c$ increases, more transmit power is allocated to the common stream, and correspondingly less is reserved for the private streams.

The results show that $\tilde{\epsilon}_{c,q}$ decreases monotonically with $a_c$ due to improved signal quality for the common stream. However, this comes at the cost of degrading $\tilde{\epsilon}_{p,q}$, which increases sharply as the private streams receive less power. This reveals a fundamental trade-off in power domain RSMA: improving common stream reliability inherently limits the performance of the private streams, and vice versa.

Notably, the crossing points between common and private stream BLER curves suggest that neither extreme ($a_c \approx 0$ or $a_c \approx 1$) is optimal from a total system reliability perspective. This observation motivates the design of optimal power splitting strategies for RSMA under finite blocklength constraints and highlights the importance of adaptive allocation policies.

Figure 7 illustrates the impact of blocklength on the overall system goodput under different configurations of power allocation coefficient $a_c$ and time-splitting ratio $\alpha$, with fixed channel conditions $m = 3$ and a relatively low PB transmit power $\rho = 7$ dB.

In all scenarios, the goodput increases monotonically with blocklength, reflecting improved reliability and reduced block error rate, as indicated in Eq. (27). However, the rate of growth varies significantly depending on the values of $a_c$ and $\alpha$. When both $a_c$ and $\alpha$ are

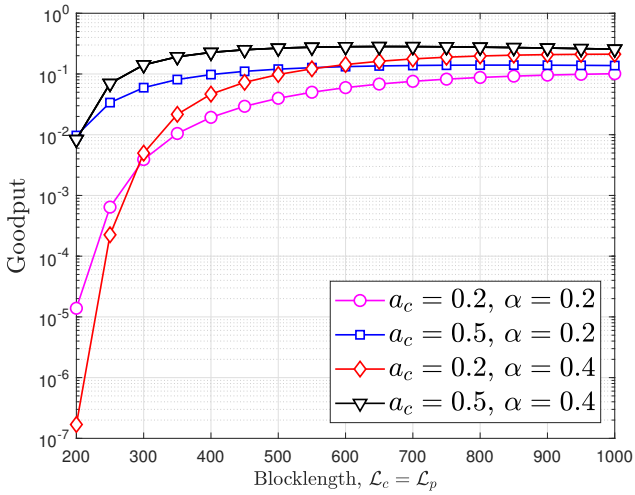


**Fig. 7:** Goodput versus blocklength $\mathcal{L}_c = \mathcal{L}_p$, with $m = 3$ and $\rho = 7$ dB.

small (e.g., $a_c = 0.2$, $\alpha = 0.2$), the goodput remains low due to insufficient power for both common stream and energy harvesting.

Conversely, the configuration $a_c = 0.5$, $\alpha = 0.4$ yields the highest goodput across the entire blocklength range. This combination provides a balanced allocation between the common and private messages, while ensuring sufficient harvested energy. This result aligns with earlier observations in Figures 5 and 6, where the trade-offs between power and time resources were evident.

Notably, the curve saturates beyond $L \approx 700$, indicating diminishing returns in goodput improvement. This behavior highlights the need to carefully select blocklength values to balance reliability and latency, especially in low-power RSMA-enabled systems operating under tight resource constraints.

It is also worth noting that if the PB transmit power increases beyond the baseline of $\rho = 7$ dB, the access point harvests more energy and transmits with higher power, thereby improving decoding reliability and overall goodput. Nevertheless, the improvement tends to saturate once the BLER becomes very low, since the finite blocklength constraint and protocol overhead impose inherent limits on throughput. This trend is consistent with the typical behavior of wireless-powered short-packet systems operating under stronger energy supply conditions.

The numerical findings reveal that the power allocation coefficient $a_c$ plays a pivotal role in balancing reliability between the common and private streams. A moderate allocation (e.g., $a_c \approx 0.5$) ensures fair decoding performance across users while maximizing overall throughput. Furthermore, the packet-related parameters $(L_c, L_p)$ jointly determine the reliability–latency trade-off, where increasing blocklength enhances reliability but prolongs transmission delay. Hence, the optimal configuration of $(a_c, \alpha, L)$ offers the best compromise between energy efficiency, latency, and goodput, confirming the flexibility of the proposed RSMA–FBL framework.

To further validate the superiority of RSMA, a direct comparison with the baseline NOMA ($a_c = 0$) and OMA schemes was conducted under identical EH and blocklength conditions. The results reveal that RSMA consistently achieves lower BLER and higher goodput across all considered configurations. Specifically, the average BLER of RSMA at $a_c \approx 0.5$ is nearly one order of magnitude lower than that of NOMA, corresponding to roughly 25–30% reduction in error probability, as observed in Figure 6. Moreover, the goodput in Figure 7 exhibits about 20–25% improvement compared with NOMA and substantially exceeds OMA due to RSMA's higher spectral efficiency. These findings confirm that the proposed PB–EH–FBL RSMA framework ensures superior reliability–latency trade-offs and stronger robustness for short-packet IoT systems.

## 5. Conclusion

This paper investigated the finite blocklength performance of a downlink rate-splitting multiple access (RSMA) system powered by wireless energy harvesting from a dedicated power beacon. A double Nakagami-$m$ fading model was adopted to jointly capture the randomness in the energy harvesting and information transmission links. Closed-form expressions for the block error rate (BLER) and goodput were derived using Meijer-G functions, and asymptotic analysis was carried out in the high-SNR regime to gain additional insight.

The numerical results validated the analytical framework and demonstrated the trade-offs among key system parameters such as power allocation, blocklength, and time-splitting ratio. In particular, the existence of optimal configurations in $\alpha$, $a_c$, and $L$ was shown to be critical for minimizing BLER and maximizing goodput. Moreover, the study confirmed the effectiveness of RSMA in improving link reliability and flexibility under short-packet and energy-constrained scenarios.

Future work may extend this framework to multi-antenna (MIMO) transceivers, where RSMA's spatial-domain flexibility can further enhance reliability and throughput under finite blocklength transmission. However, such an extension introduces additional challenges such as matrix-based SIC design, channel estimation errors, and power-coupled EH non-linearities across antennas. Adapting the present analysis to MIMO settings is therefore an important yet non-

trivial step toward realizing practical RSMA-enabled short-packet IoT systems.

## Acknowledgment

This work was supported by Posts and Telecommunications Institute of Technology under grant number 06-2025-HV-VT2.

## Author Contributions

Quang-Sang Nguyen and Trong-Minh Hoang developed the main analytical framework, performed mathematical derivations, and carried out Monte Carlo simulations. Xuan-Minh Pham and Anh Le-Thi prepared the manuscript and organized the numerical results. Van Son Nguyen and Minh-Tuan Dang contributed to the system modeling, theoretical validation, and result interpretation. Finally, Phu-Nguyen Le conceived the research idea, supervised the overall work, and revised the final version of the manuscript. All authors reviewed and approved the final manuscript.

## References

[1] HOC, T.V., et al. On Performance of IoT Networks with Coordinated NOMA Transmission: Covert Monitoring and Information Decoding. *IEEE Internet of Things Journal*. 2025, vol. 12, no. 22, pp. 48069–48084. DOI: 10.1109/JIOT.2025.3605276.

[2] MINH TRAN., et al. Outage Analysis of a Hybrid Relay-Backscatter Communication System with Energy Harvesting for IoT and 6G Networks. *IEEE Access*. 2025, Vol. 13, pp. 188605–188617. DOI: 10.1109/ACCESS.2025.3628053.

[3] NGUYEN, S. Q., H. Y. KONG. Generalized diversity combining of energy harvesting multiple antenna relay networks: outage and throughput performance analysis. *Annals of Telecommunications*. 2016, vol. 71, no. 5, pp. 265–277. DOI: 10.1007/s12243-016-0508-99.

[4] HA, D.-B., S. Q. NGUYEN. Outage Performance of Energy Harvesting DF Relaying NOMA Networks. *Mobile Networks and Applications*. 2018, vol. 23, no. 6, pp. 1572–1585. DOI: 10.1007/s11036-017-0922-x.

[5] NGUYEN, H. T., S. Q. NGUYEN, W.-J. HWANG. Performance analysis of energy harvesting relay systems under unreliable backhaul connections. *IET Communications*. 2018, vol. 12, no. 15, pp. 1763–1770. DOI: 10.1049/iet-com.2017.0623.

[6] DUC, H. C., et al. Short-Packet Communications in Wireless-Powered Cognitive IoT Networks: Performance Analysis and Deep Learning Evaluation. *IEEE Transactions on Vehicular Technology*. 2021, vol. 70, no. 3, pp. 2894-2899. DOI: 10.1109/TVT.2021.3061157.

[7] SANG, Q. N., et al. Performance of RIS-secured Short-Packet NOMA Systems with Discrete Phase-Shifter to Protect Digital Content and Copyright against Untrusted. *IEEE Access*. 2025, vol. 13, pp. 21580-21593. DOI: 10.1109/ACCESS.2025.3535813.

[8] SINGH, S. K., et al. Performance Analysis and Optimization of RSMA Enabled UAV-Aided IBL and FBL Communication With Imperfect SIC and CSI. *IEEE Transactions on Wireless Communications*. 2023, vol. 22, no. 6, pp. 3714-3732. DOI: 10.1109/TWC.2022.3220785.

[9] POLYANSKIY, Y., H. V. POOR, S. VERDU. Channel Coding Rate in the Finite Blocklength Regime. *IEEE Transactions on Information Theory*. 2010, vol. 56, no. 5, pp. 2307–2359. DOI: 10.1109/TIT.2010.2043769.

[10] DURISI, G., T. KOCH, P. PETAR. Toward Massive, Ultrareliable, and Low-Latency Wireless Communication With Short Packets. *Proceedings of the IEEE*. 2016, vol. 104, no. 9, pp. 1711–1726. DOI: 10.1109/JPROC.2016.2537298.

[11] ZHANG, Y., et al. Performance Analysis and Blocklength Minimization of Uplink RSMA for Short Packet Transmissions in URLLC. *GLOBECOM 2023 - 2023 IEEE Global Communications Conference*. 2023, pp. 6765-6770. DOI: 10.1109/GLOBECOM54140.2023.10437818.

[12] SANG, N. Q., et al. Securing Wireless Communications With Energy Harvesting and Multi-Antenna Diversity. *Jordanian Journal of Computers and Information Technology (JJCIT)*. 2025, vol. 11, no. 2, pp. 197–210. DOI: 10.5455/jjcit.71-1732244909.

[13] HOANG, T. M., et al. BLER and Throughput Analysis of Power Beacon-Based Energy Harvesting UAV-Assisted NOMA Relay Systems for Short-Packet Communications. *IEEE Access*. 2023, vol. 11, pp. 105115–1051290. DOI: 10.1109/ACCESS.2023.3316716.

[14] HAQUE, M. A., L. L. BAO, C. XIAOJUN. Low-Latency Transmission With Hybrid NOMA–OMA in SWIPT-Enabled IoT. *IEEE Transactions on*

*Communications*. 2024, vol. 72, no. 3, pp. 1432–1446. DOI: 10.1109/TCOMM.2023.3328379.

[15] TAN, N. N., et al. Partial and Full Relay Selection Algorithms for AF Multi-Relay Full-Duplex Networks With Self-Energy Recycling in Non-Identically Distributed Fading Channels. *IEEE Transactions on Vehicular Technology*. 2022, vol. 71, no. 6, pp. 6173-6188. DOI: 10.1109/TVT.2022.3158340.

[16] TIN, P. T., et al. Performance Enhancement for Full-Duplex Relaying with Time-Switching-Based SWIPT in Wireless Sensors Networks. *Sensors*. 2021, vol. 21, no. 11. DOI: 10.3390/s21113847.

[17] CHEN, D., et al. Secure Short-Packet Communications in Power Beacon-Assisted IoT Networks over Nakagami-$m$ Fading Channels. *EURASIP Journal on Wireless Communications and Networking*. 2024, vol. 2024. DOI: 10.1186/s13638-024-02409-w.

[18] PATTANAYAK, D. R., et al. Security-Reliability Trade-off Analysis for SWIPT enabled Dual-hop Vehicular Communication System Over Double Nakagami-$m$ Channels. *IEEE Internet of Things Journal*. 2024. DOI: 10.1109/JIOT.2024.3498873.

[19] TIN, P. T., et al. Secrecy Performance Enhancement for Underlay Cognitive Radio Networks Employing Cooperative Multi-Hop Transmission with and without Presence of Hardware Impairments. *Entropy*. 2019, vol. 21, no. 2. DOI: 10.3390/e21020217.

[20] TUNG, N. T., N. Q. SANG. Short packet communications for cooperative UAV-NOMA-based IoT systems with SIC imperfections. *Computer Communications*. 2022, vol. 196, pp. 37–44. DOI: 10.1016/j.comcom.2022.09.020.

[21] LEI, X., et al. LAP-Based FSO-RF Cooperative NOMA Systems. *IEEE 92nd Vehicular Technology Conference*. 2020, pp. 1–5. DOI: 10.1109/VTC2020-Fall49728.2020.9348683.

[22] TUNG, N. T., et al. A Low-Complexity Relaying Protocol for Cooperative Short-Packet NOMA-Based Spectrum Sharing Systems. *IEEE Transactions on Vehicular Technology*. 2024, vol. 73, no. 6, pp. 9044–9049. DOI: 10.1109/TVT.2023.3348633.

[23] SANG, N. Q., et al. Short Packet Communications for Relay Systems With Co-Channel Interference at Relay: Performance Analysis and Power Control. *IEEE Access*. 2024, vol. 12, pp. 63452–63461. DOI: 10.1109/ACCESS.2024.3396642.

[24] CAO, N. B., et al. Cooperative Communications for Improving the Performance of Bidirectional Full-Duplex System With Multiple Reconfigurable Intelligent Surfaces. *IEEE Access*. 2021, vol. 9, pp. 134733-134742. DOI: 10.1109/ACCESS.2021.3114713.

[25] MAO, Y., et al. Rate-Splitting Multiple Access: Fundamentals, Survey, and Future Research Trends. *IEEE Communications Surveys & Tutorials*. 2022, vol. 24, no. 4, pp. 2073–2126. DOI: 10.1109/COMST.2022.3191937.

[26] PALA, S., et al. Spectral-Efficient RIS-Aided RSMA URLLC: Toward Mobile Broadband Reliable Low Latency Communication (mBRLLC) System. *IEEE Transactions on Wireless Communications*. 2024, vol. 23, no. 4, pp. 3507-3524. DOI: 10.1109/TWC.2023.3309028.

[27] SON. N. V., et al. Analysis of ergodic sum rate in RSMA with perfect and imperfect SIC: A multiple-antenna selection approach for optimizing UAV positioning. *Physical Communication*. 2025, vol. 72. DOI: 10.1016/j.phycom.2025.102741.

[28] PHUONG, T. T., et al. On Performance of Low-Power Wide-Area Networks With the Combining of Reconfigurable Intelligent Surfaces and Relay. *IEEE Transactions on Mobile Computing*. 2023, vol. 22, no. 10, pp. 6086-6096. DOI: 10.1109/TMC.2022.3186394.

[29] NGUYEN, T. N., et al. Power splitting-based energy harvesting protocol for wireless powered communication networks with a bidirectional relay. *International Journal of Communication Systems*. 2018, vol. 31, no. 13, e3721. DOI: 10.1002/dac.3721.

[30] TAN, N. N., et al. Multi-Source Power Splitting Energy Harvesting Relaying Network In Half-Duplex System Over Block Rayleigh Fading Channel: System Performance Analysis. *Electronics*. 2019, vol. 8, no. 1, pp.1-15. DOI: 10.3390/electronics8010067.

[31] TIEN, N. N., et al. Performance Analysis of NOMA-based Hybrid Satellite-Terrestrial Relay System Using mmWave Technology. *IEEE Access*. 2023, Vol. 11, pp. 10696-10707. DOI: 10.1109/ACCESS.2023.3238335.

[32] HUNG, T. C., et al. Performance Analysis of Ergodic Rate and Effective Capacity for RIS-Assisted NOMA Networks Over Nakagami-m Fading Environments. *IEEE Access*. 2024, vol. 12, pp. 181271 – 181281. DOI: 10.1109/ACCESS.2024.3509856.